Electronics and Information Technologies, 2026, 35, 109–120
http://publications.lnu.edu.ua/collections/index.php/electronics/index

UDC 004.852:004.942:621.73

SURROGATE MODELING OF ELASTIC-PLASTIC SHEET METAL BENDING: A COMPARATIVE STUDY OF SURROGATE METHODS AND A DIAGNOSTIC TEST OF PHYSICS REGULARIZATION

Bohdan Petrovskyi
Department of Applied Mathematics,
Ivan Franko National University of Lviv,
1 Universytetska Street, Lviv, 79007, UKRAINE

Petrovskyi, B. (2026). Surrogate Modeling of Elastic-Plastic Sheet Metal Bending: A Comparative Study of Surrogate Methods and a Diagnostic Test of Physics Regularization. *Electronics and Information Technologies*, 35, 109–120. https://doi.org/10.30970/eli.35.8

ABSTRACT

Background. Sheet metal bending is a key manufacturing operation in which springback — the partial elastic recovery of the workpiece after unloading — causes deviations from the target geometry and must be predicted accurately. Repeated finite element simulations are computationally expensive for wide parametric studies, motivating fast surrogate models. This work compares surrogate modeling approaches for elastic-plastic sheet bending and evaluates the diagnostic value of a physics consistency check for detecting physically implausible neural surrogates, independently of whether physics regularization improves raw predictive accuracy.

Methods. A dataset of 39 568 finite element simulations was generated in COMSOL Multiphysics 6.2 by varying sheet thickness, punch displacement, and Young's modulus of a 6111-T4 aluminum alloy blank. Five classical surrogate methods and three neural network models (a pure data-driven baseline, a Hollomon-regularized model with correct parameters, and a control model with intentionally incorrect parameters) were compared over 5 random data splits. A sensitivity sweep varied the control model's hardening exponent between the true and the incorrect value to test how sharply the diagnostic responds.

Results. Classical non-parametric methods slightly outperform the neural surrogates on the dense smooth parameter grid: the random forest achieves a coefficient of determination of $R^2 > 0.9999$, compared to $R^2 \approx 0.999$ for the neural models. Differences in raw accuracy among the three neural models are statistically detectable across seeds (paired t-test) but tiny in magnitude ($\Delta R^2 < 0.1$ percentage point). The physics consistency metric, in contrast, separates the models by orders of magnitude: $R^2 = 0.999$ for the correct model versus $R^2 \approx -2.9$ for the incorrect one. The sensitivity sweep reveals a sharp threshold rather than gradual degradation: consistency remains near-perfect while the hardening exponent error stays small, then collapses once the exponent deviates substantially from its true value.

Conclusion. Standard accuracy metrics are insufficient to detect physically inconsistent neural surrogates, and the underlying diagnostic signal is thresholded rather than gradual. The physics consistency metric provides an independent diagnostic criterion that complements standard accuracy measures.

Keywords: physics-regularized neural networks; surrogate modeling; sheet metal bending; springback; Hollomon hardening law; random forest.

© 2026 Bohdan Petrovskyi. Published by the Ivan Franko National University of Lviv on behalf of Електроніка та інформаційні технології / Electronics and information technologies. This is an Open Access article distributed under the terms of the Creative Commons Attribution 4.0 License which permits unrestricted reuse, distribution, and reproduction in any medium, provided the original work is properly cited.

1. INTRODUCTION

Sheet metal forming is one of the key technological operations in mechanical engineering, aerospace, and automotive manufacturing. A major difficulty in sheet bending is springback, i.e., the partial elastic recovery of the workpiece after the punch is retracted. Springback causes deviations between the desired and the obtained geometry and therefore requires accurate prediction during process design. The finite element method (FEM) is the standard numerical tool for such problems [1, 2], but repeated FEM simulations become computationally expensive when a wide range of technological or material parameters must be investigated.

1.1. Surrogate models for metal forming

Surrogate and data-driven models for metal forming have been studied extensively. Early work used response surface methods and kriging [5, 6]. Neural networks were applied to springback prediction in V-bending [7] and air bending [8]. More recent work has employed Gaussian process regression, support vector machines, and ensemble methods for forming process optimization [9]. Machine learning methods have also been applied to fracture mechanics [10]. A comparative study of surrogate methods for sheet forming was presented in [11]. More recently, a machine learning-driven stress integration method was developed for anisotropic plasticity in sheet metal forming [21], and comparative studies of ANN and PINN approaches for sheet metal forming continue to appear [23].

Physics-informed and physics-regularized machine learning methods [3, 4] provide a way to embed physical knowledge into data-driven models. PINNs applied to elastoplasticity [12] and neural operator methods for multiscale inelastic problems [13], as well as physics-informed modeling of finite-strain plasticity [22], represent one direction. An alternative uses soft physics-based regularization terms without requiring the full PDE residual [14, 15]. The Hollomon hardening law has been incorporated into neural networks for material parameter identification [16] and stress prediction under cyclic loading [17].

1.2. Contribution of the present work

The present paper makes two contributions, both evaluated with multi-seed statistical support. First, it introduces a fake-physics control experiment as a diagnostic tool: a model with incorrect Hollomon parameters is trained alongside the physically consistent model, showing that standard accuracy metrics (coefficient of determination, R^2, and mean absolute error, MAE) cannot reliably detect physically inconsistent models, while a physics consistency metric separates them by orders of magnitude; a sensitivity sweep further shows that this diagnostic signal is thresholded rather than gradual. Second, it provides a systematic comparison of neural surrogate models against classical non-parametric methods (RBF interpolation, random forest, polynomial regression) on a benchmark sheet bending problem, showing that classical methods remain more accurate on this smooth three-parameter problem — so the value of the proposed model lies in its diagnostic behavior rather than in a raw predictive advantage.

2. MATERIALS AND METHODS

2.1. Problem formulation

The problem is a 2D plane-strain cross-section of a sheet metal bending process. The input vector is defined as:

$$\mathbf{x} = (t, \delta, E)^T \in \mathbb{R}^3, \tag{1}$$

where:

- t is sheet thickness (mm);
- δ is maximum punch displacement (mm);

- E is Young's modulus (GPa).

The output vector is defined as:

$$\mathbf{y} = (\sigma_{max}, u_{max}, \theta)^T \in \mathbb{R}^3, \tag{2}$$

where:

- σ_{max} is maximum von Mises stress (Pa);
- u_{max} is maximum displacement (m);
- θ is final bending angle after springback (° – deg).

2.2. FEM model for data generation

FEM simulations were performed in COMSOL Multiphysics 6.2 (Solid Mechanics module) using the benchmark sheet metal forming configuration [20], automated via a MATLAB script through the COMSOL LiveLink interface. The geometry is a 2D cross-section exploiting bilateral symmetry: a deformable sheet (L = 60 mm, w = 30 mm), a rigid punch (R_1 = 23.5 mm), and a rigid die (R_2 = 25 mm, shoulder R_3 = 4 mm, width 50 mm).

The blank is a 6111-T4 aluminum alloy with E_0 = 70.5 GPa, ν = 0.34, ρ = 2700 kg/m³, σ_0 = 194 MPa. Young's modulus E is varied as an input. Plastic hardening follows the Hollomon power law:

$$\sigma_{eq} = K \cdot \varepsilon_{np}, \quad K > 0, \quad n > 0, \tag{3}$$

with K = 550.4 MPa and n = 0.223 for the reference alloy. Friction coefficient μ = 0.1342; contact enforced with the augmented Lagrangian method [19]. The contact non-penetration conditions are:

$$g_n \geq 0, \quad \sigma_n \leq 0, \quad g_n \sigma_n = 0; \quad |\tau| \leq \mu |\sigma_n|. \tag{4}$$

These equations govern only the FEM simulations and are not imposed as residuals in the neural network loss.

2.3. Dataset construction

The dataset was assembled from multiple simulation runs with parameter ranges: $t \in [0.45, 1.50]$ mm, $\delta \in [18.0, 28.5]$ mm, $E \in [55.5, 175.5]$ GPa. The FEM solver advances the punch displacement through a monotonic arc-length continuation parameter; a run is retained only if this parameter reaches at least 0.95 of its target value, confirming that the solver tracked the loading path to (near-)completion without losing convergence. Runs that stalled below this threshold, typically for extreme parameter combinations that induce severe contact/plasticity nonlinearity, were discarded as non-converged rather than kept as unreliable partial solutions. The retained dataset contains N = 39 568 samples, all with von Mises stress above σ_0 = 194 MPa. The dataset is divided into training / validation / test (80% / 10% / 10%: 31 654 / 3 957 / 3 957 samples). Variables are standardized using statistics computed only on the training subset.

The raw von Mises stress exported via COMSOL LiveLink for MATLAB was rescaled by a fixed multiplicative factor to express MaxVonMises in SI Pascals, consistent with the units used for the Hollomon hardening parameters (K = 550.4 MPa) throughout the pipeline. This scaling was applied uniformly to the entire dataset before any train/validation/test split and before computing any of the standardization statistics above; it therefore does not affect relative comparisons (R^2, MAE, physics consistency) between surrogate models, only the absolute stress scale reported.

The Young's modulus range intentionally extends well beyond the physically realistic range for 6111-T4 aluminum (E_0 = 70.5 GPa) and partly overlaps typical values for steel. This was a deliberate choice to probe the surrogate's response surface over a wide input range, rather than to represent a physically realistic material variation; the corresponding predictions should be read as a numerical sensitivity study of the input–output map, not as material-specific forecasts outside the aluminum alloy's true elastic range.

2.4. Surrogate methods

Classical baselines. Five classical methods are evaluated:

1. Linear regression (multi-output OLS).
2. Polynomial regression of degree 2 (scikit-learn Pipeline).
3. Polynomial regression of degree 3 (scikit-learn Pipeline).
4. RBF interpolation — thin-plate spline (scipy RBFInterpolator, smoothing 10^{-3}), analogous to kriging.
5. Random forest — 300 regression trees (scikit-learn RandomForestRegressor).

Neural network baseline (Pure ML). Two hidden layers of 64 neurons, Swish activation, dropout 0.1, L^2 regularization 10^{-4}. Training: Adam (lr = 5×10^{-4}), batch 64, early stopping (patience 15), max 120 epochs.

Soft Hollomon-regularized model. Augments the network with a latent output $\hat{\varepsilon}_p$ (softplus-constrained). The total loss is:

$$\mathcal{L}_{\text{total}} = \mathcal{L}_{\text{data}} + \lambda_{\text{phys}}\mathcal{L}_{\text{phys}} + \alpha\mathcal{L}_{\text{bound}} + \beta\|\theta\|^2, \tag{5}$$

where $\mathcal{L}_{\text{phys}}$ penalizes the discrepancy between $\hat{\sigma}_{max}$ and Hollomon stress $\sigma_H = K(\hat{\varepsilon}_p + \varepsilon)^n$, normalized by s_σ. Penalty $\mathcal{L}_{\text{bound}}$ keeps $\hat{\varepsilon}_p \in [\varepsilon_{min}, \varepsilon_{max}]=[10^{-5}, 0.05]$. λ_{phys} annealed from 0 to 0.5; α = 10, β = 10^{-4}. Training: 25 pretraining + 80 physics-regularized epochs. Stress rescaled for numerical stability; $\hat{\varepsilon}_p$ is a numerically effective parameter, not the physical plastic strain.

The latent output $\hat{\varepsilon}_p$ is produced by a separate one-unit dense head with a softplus activation; this head shares the same two-layer trunk and the same input vector $\mathbf{x}$ as the three main output heads and receives no additional information.

The physics consistency metrics reported in Section 3.2 are defined as:

$$Physics\ MAE = \frac{1}{N}\sum_i |\sigma_{H,i} - \hat{\sigma}_{max,i}|, \tag{6}$$

$$Physics\ R^2 = 1 - \sum_i \left(\sigma_{H,i} - \hat{\sigma}_{max,i}\right)^2 \Big/ \sum_i \left(\sigma_{H,i} - \bar{\sigma}_H\right)^2, \tag{7}$$

$$Rel.error = \frac{1}{N}\sum_i |\hat{\sigma}_{max,i} - \hat{\sigma}_{H,i}|/(\sigma_{H,i} + \varepsilon), \tag{8}$$

where $\bar{\sigma}_H$ is the mean of σ_H over the test set and $\varepsilon = 10^{-6}$ avoids division by zero. All three compare the network's predicted stress $\hat{\sigma}_{max}$ against the Hollomon stress $\sigma_H = K(\hat{\varepsilon}_p + \varepsilon)^n$ implied by its own latent strain, over the N test-set samples.

Fake Hollomon control. Same as above but $n_{\text{fake}} = 0.8$ instead of $n = 0.223$ (K retained). Tests whether an inconsistent physical constraint degrades predictive accuracy.

Implementation. TensorFlow 2.x, Google Colaboratory (GPU); scikit-learn 1.8, scipy 1.17. Unless noted otherwise, the values shown are the mean over 5 independent random data splits (seeds 42, 123, 2024, 7, 2025); the training-fraction sensitivity (**Table 4**) and the fake-physics sensitivity sweep (Section 3.3) average over 3 of these seeds (42, 123, 2024), and all other single-model results use seed 42.

3. RESULTS AND DISCUSSION

3.1. Comparison of all surrogate methods

Table 1 reports R^2 values and bending angle MAE for all methods, averaged over 5 seeds ($N = 3\,957$ per split). **Table 2** shows MAE for all three outputs. RBF and random forest substantially outperform the neural models. The random forest attains $R^2 > 0.9999$ with angle MAE = 0.001°, compared to 0.273–0.289° for the neural models. The RBF interpolant achieves $R^2 = 0.9999$, angle MAE = 0.073°. Neural models match or slightly exceed polynomial regression of degree 2 and 3, confirming that the neural surrogate is a reasonable choice in higher-dimensional settings but does not outperform well-chosen non-parametric baselines on this three-parameter smooth problem.

Table 1. **Test R^2 and bending angle MAE ($N = 3\,957$, 10% split)**

Method	σ_{max} R^2	u_{max} R^2	θ R^2	θ MAE (°)
Linear regression	0.9982	0.9884	0.9978	0.598
Polynomial (deg. 2)	0.9992	0.9990	0.9994	0.301
Polynomial (deg. 3)	0.9993	0.9994	0.9997	0.222
RBF (thin-plate spline)	1.0000	0.9999	0.9999	0.073
Random forest (300 trees)	1.0000	1.0000	1.0000	0.001
Neural net (Pure ML)	0.9991	0.9992	0.9995	0.281
+ Hollomon (true K, n)	0.9990	0.9993	0.9995	0.273
+ Hollomon (fake $n = 0.8$)	0.9987	0.9992	0.9995	0.289

Table 2. **Mean absolute errors (MAE) for all surrogate methods on the test set**

Method	σ_{max} MAE (Pa)	u_{max} MAE (m)	θ MAE (°)
Linear regression	1.44×10^{6}	2.50×10^{-4}	0.598
Polynomial (deg. 2)	6.42×10^{5}	6.88×10^{-5}	0.301
Polynomial (deg. 3)	6.16×10^{5}	5.26×10^{-5}	0.222
RBF (thin-plate spline)	4.34×10^{4}	1.49×10^{-5}	0.073
Random forest (300 trees)	4.25×10^{3}	2.39×10^{-7}	0.001
Neural net (Pure ML)	7.59×10^{5}	6.45×10^{-5}	0.281
+ Hollomon (true K, n)	8.61×10^{5}	5.95×10^{-5}	0.273
+ Hollomon (fake $n = 0.8$)	1.00×10^{6}	6.52×10^{-5}	0.289

3.2. Physical consistency

Although all three neural models achieve comparable predictive accuracy, they differ substantially in physical consistency. **Table 3** compares the predicted stress $\hat{\sigma}_{\max}$ with the Hollomon stress σ_H computed from the latent output. To test how sharply this diagnostic responds to the degree of physical inconsistency, the control model was retrained with the hardening exponent n swept between the true value (0.223) and the fake value (0.8), on 3 seeds per value.

Table 3. **Physical consistency vs. hardening exponent *n* used in the control model (*mean* ± *std* over 3 seeds: 42, 123, 2024). True value *n* = 0.223; fake control *n* = 0.8**

Hollomon exponent n	*Physics* MAE (Pa)	*Physics* R^2	*Rel. error*
n = 0.223 (true)	1.43×10⁶ ± 5.4×10⁵	0.999 ± 0.001	1.0% ± 0.4%
n = 0.35	1.07×10⁶ ± 6.4×10⁵	0.999 ± 0.002	0.7% ± 0.4%
n = 0.5	8.26×10⁷ ± 4.3×10⁷	−5.25 ± 4.66	35.2% ± 8.5%
n = 0.65	4.34×10⁷ ± 3.4×10⁶	−1.48 ± 0.40	33.1% ± 3.5%
n = 0.8 (fake)	5.51×10⁷ ± 3.8×10⁵	−2.90 ± 0.65	67.0% ± 4.1%

Averaged over 3 seeds, the model with the correct exponent achieves physics R^2 = 0.999±0.001 and relative error 1.0%±0.4%, while the fake-physics control (n = 0.8) achieves *Physics* R^2 = −2.90±0.65 and *Relative error* 67.0%±4.1% (**Table 3**). The sensitivity sweep reveals a sharp threshold rather than a gradual decline: consistency remains near-perfect at n = 0.35 (*Physics* R^2 = 0.999±0.002), a 57% *Relative error* in the exponent itself, but collapses once n reaches 0.5 (*Physics* R^2 = −5.25±4.66) and stays poor thereafter. The latent strain for the true model is consistent with the FEM benchmark observation of ≈2% maximum equivalent plastic strain [20]; for $n \geq 0.5$ the latent strain substantially exceeds the soft upper bound $\varepsilon_{max} = 0.05$. **Fig. 1** and **Fig. 2** illustrate the scatter and loss histories for the true and fake endpoints.

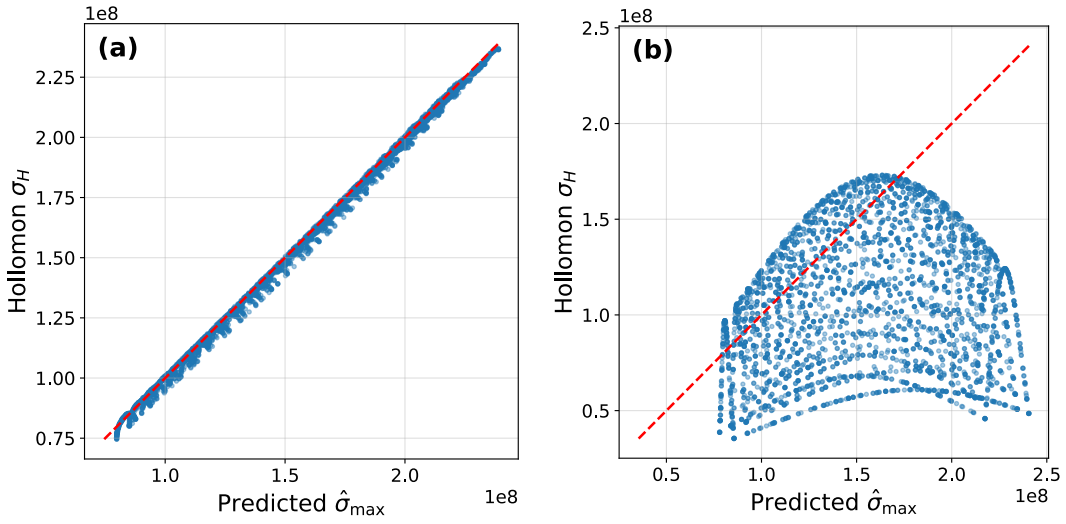


Fig. 1. Predicted stress $\hat{\sigma}_{max}$ vs. Hollomon stress σ_H: (a) true K, n; (b) fake $n = 0.8$. Dashed line — perfect agreement

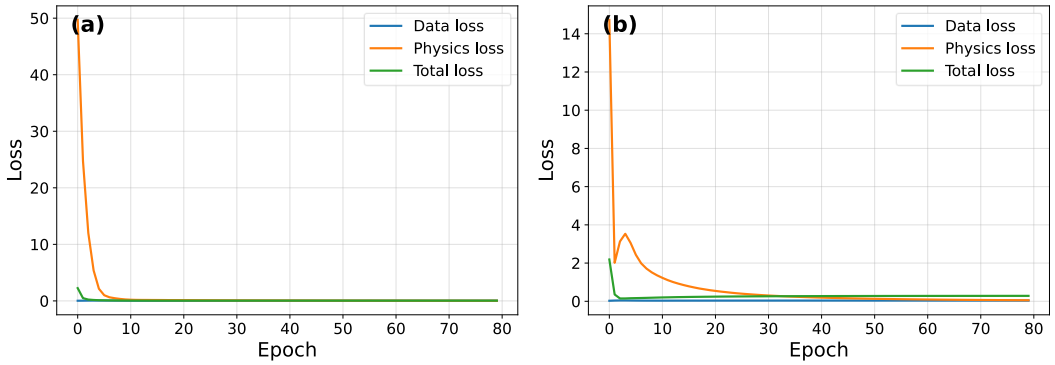


Fig. 2. Training loss histories: (a) true model; (b) fake model. Physics loss (orange) plateaus higher for the fake model

3.3. Accuracy does not imply physical consistency

All three neural models achieve $R^2 \approx 0.999$ regardless of whether the Hollomon parameters are correct, incorrect, or absent. Differences in raw accuracy across the three models are statistically detectable over 5 seeds (paired t-test on R^2 of σ_{max}: Pure ML vs. true-Hollomon, $p = 0.22$, not significant; Pure ML vs. fake-Hollomon, $p = 0.014$; true- vs. fake-Hollomon, $p = 0.016$) but are tiny in absolute magnitude ($\Delta R^2 < 0.1$ percentage point) and practically negligible for model selection based on accuracy alone. This illustrates a general risk in data-driven modeling: high predictive accuracy does not guarantee physical consistency [4]. The physics consistency metric (**Table 3**), in contrast, separates the models by orders of magnitude and remains diagnostic across a wide range of hardening-exponent perturbations.

3.4. Sensitivity to training set size

Table 4 shows mean R^2 over 3 seeds for training fractions from 5% to 100%. Standard deviation $\sigma < 0.001$ in all entries; maximum $\sigma = 0.0007$ (u_{max}, Hollomon, 5%). **Fig. 3** illustrates the results.

Both models maintain $R^2 \approx 0.999$ across all fractions. The pure neural network is marginally more stable at 5–10%, while the Hollomon model catches up from 25% onward. Physics regularization does not provide a clear advantage in data efficiency.

Table 4. **Mean test R^2 over 3 seeds vs. training fraction. Max $\sigma = 0.0007$ (u_{max}, Hollomon, 5%); all other entries: $\sigma < 0.0005$**

Output	Model	5%	10%	25%	50%	100%
σ_{max}	Pure ML	0.9989	0.9989	0.9989	0.9990	0.9989
	Hollomon	0.9983	0.9983	0.9988	0.9989	0.9989
u_{max}	Pure ML	0.9989	0.9991	0.9992	0.9993	0.9992
	Hollomon	0.9974	0.9985	0.9991	0.9993	0.9993
θ	Pure ML	0.9993	0.9995	0.9995	0.9994	0.9995
	Hollomon	0.9989	0.9991	0.9995	0.9995	0.9995

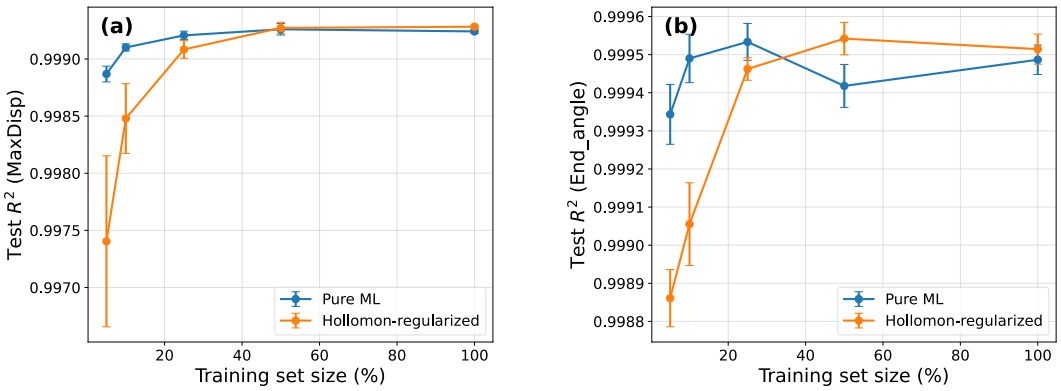


Fig. 3. Test R² vs. training set size (*mean* ± *std*, 3 seeds): (a) u_{max}; (b) θ

3.5. When classical baselines are competitive

RBF and random forest outperform the neural surrogate on this problem [11, 18]. This is consistent with known behavior for smooth low-dimensional response surfaces on regular grids. The neural surrogate would offer advantages for higher input dimensionality (e.g., including Poisson's ratio, friction coefficient, tool geometry), irregular sampling, or when explicit physical constraints on outputs are required.

3.6. Interpretation of the Hollomon regularization

The Hollomon regularization links the predicted maximum von Mises stress to a latent scalar strain through a global power law. In a real bending problem, the stress distribution is nonuniform and the maximum stress is not uniquely determined by the scalar Hollomon law at a single representative strain. The latent strain $\hat{\varepsilon}_p$ is therefore an effective model parameter, not a physically measurable quantity, and is not validated against FEM plastic strain fields. Nevertheless, the fake-physics experiment confirms that the physics consistency check is informative.

3.7. Limitations

The following limitations apply:

1. Dataset generated numerically; accuracy bounded by FEM fidelity.
2. Latent plastic strain not validated against FEM fields.
3. Only global scalar quantities predicted; no field reconstruction.
4. Neural surrogate does not outperform classical baselines on this smooth three-parameter problem.
5. Dataset grid is non-uniform across simulation runs.
6. Extrapolation outside the parameter range is not assessed.

4. CONCLUSIONS

A systematic comparison of surrogate modeling methods for elastic-plastic sheet metal bending has been presented. Five classical methods and three neural network models were evaluated on a dataset of 39 568 FEM simulations. The main findings are:

1. Classical baselines outperform neural surrogates on the dense smooth parameter grid. The random forest attains $R^2 > 0.9999$, the RBF interpolant $R^2 = 0.9999$, compared to $R^2 \approx 0.999$ for the neural models.
2. Physics regularization does not improve data efficiency: both pure and Hollomon-regularized models maintain comparable accuracy across training set fractions from 5% to 100%.

3. Standard accuracy metrics cannot detect physically inconsistent models. Over 3 seeds, the fake-physics control exhibits 67.0% ± 4.1% physics consistency error and physically unrealistic latent strain values, while the correct model achieves 1.0% ± 0.4% physics error. Differences in raw predictive accuracy among the three neural models, while statistically detectable across seeds, are tiny in absolute magnitude ($\Delta R^2 < 0.1$ percentage point); the physics consistency metric, in contrast, separates them by orders of magnitude.
4. The diagnostic signal is thresholded, not gradual. A sensitivity sweep over the control model's hardening exponent shows that physics consistency remains near-perfect while the exponent error stays below ~57% of its true value, then collapses sharply once the error grows further — a practical implication for how large a parameter mismatch this diagnostic can be expected to catch.

ACKNOWLEDGMENTS AND FUNDING SOURCES

The author expresses sincere gratitude to Andrii Pereimybida, Associate Professor at the Department of Applied Mathematics, Ivan Franko National University of Lviv, for helpful consultations, discussion of the manuscript structure, and assistance with interpreting the results.

The author received no financial support for the research, writing, and publication of this article.

COMPLIANCE WITH ETHICAL STANDARDS

The author declares that the research was conducted in the absence of any conflict of interest.

CODE AND DATA AVAILABILITY.

The Python training/analysis code is available at https://colab.research.google.com/drive/1ys2mN5-h_uRl6N6BzixdI7aaAY8sEjT7?usp=sharing. The COMSOL model, MATLAB data-generation script, and raw simulation dataset are available from the author upon reasonable request.

Author has read and agreed to the published version of the manuscript.

REFERENCES

[1] Belytschko, T., Liu, W. K., Moran, B., & Elkhodary, K. (2014). *Nonlinear finite elements for continua and structures* (2nd ed.). Wiley. https://www.wiley.com/en-us/Nonlinear+Finite+Elements+for+Continua+and+Structures,+2nd+Edition-p-9781118632703

[2] Zienkiewicz, O. C., & Taylor, R. L. (2005). *The finite element method* (5th ed.). Butterworth-Heinemann. https://doi.org/10.1016/B978-075066431-8.50196-X

[3] Raissi, M., Perdikaris, P., & Karniadakis, G. E. (2019). Physics-informed neural networks: A deep learning framework for solving forward and inverse problems involving nonlinear partial differential equations. *Journal of Computational Physics*, *378*, 686–707. https://doi.org/10.1016/j.jcp.2018.10.045

[4] Karniadakis, G. E., Kevrekidis, I. G., Lu, L., Perdikaris, P., Wang, S., & Yang, L. (2021). Physics-informed machine learning. *Nature Reviews Physics*, *3*(6), 422–440. https://doi.org/10.1038/s42254-021-00314-5

[5] Naceur, H., Ben-Elechi, S., Batoz, J. L., & Knopf-Lenoir, C. (2008). Response surface methodology for the rapid design of aluminum sheet metal forming parameters. *Materials & Design*, *29*(4), 781–790. https://doi.org/10.1016/j.matdes.2007.01.018
[6] Breitkopf, P., Naceur, H., Rassineux, A., & Villon, P. (2005). Moving least squares response surface approximation: Formulation and metal forming applications. *Computers & Structures*, *83*(17–18), 1411–1428. https://doi.org/10.1016/j.compstruc.2004.07.011
[7] Kazan, R., Firat, M., & Tiryaki, A. E. (2009). Prediction of springback in wipe-bending process of sheet metal using neural network. *Materials & Design*, *30*(2), 418–423. https://doi.org/10.1016/j.matdes.2008.05.033
[8] Inamdar, M. V., Date, P. P., & Desai, U. B. (2000). Studies on the prediction of springback in air vee bending of metallic sheets using an artificial neural network. *Journal of Materials Processing Technology*, *108*(1), 45–54. https://doi.org/10.1016/S0924-0136(00)00588-4
[9] Spathopoulos, S. C., & Stavroulakis, G. (2020). Springback prediction in sheet metal forming using FEA and ANN. *Applied Mechanics*, *1*(2), 97–110. https://doi.org/10.3390/applmech1020007
[10] Liu, X., Athanasiou, C. E., Padture, N. P., Sheldon, B. W., & Gao, H. (2020). A machine learning approach to fracture mechanics problems. *Acta Materialia*, *190*, 105–112. https://doi.org/10.1016/j.actamat.2020.03.016
[11] Hamdaoui, M., Le Quilliec, G., Breitkopf, P., & Villon, P. (2014). POD surrogates for real-time multi-parametric sheet metal forming problems. *International Journal of Material Forming*, *7*(3), 337–358. https://doi.org/10.1007/s12289-013-1132-0
[12] Haghighat, E., Raissi, M., Moure, A., Gomez, H., & Juanes, R. (2021). A physics-informed deep learning framework for inversion and surrogate modeling. *Computer Methods in Applied Mechanics and Engineering*, *379*, 113741. https://doi.org/10.1016/j.cma.2021.113741
[13] Yin, M., Zhang, E., Yu, Y., & Karniadakis, G. E. (2022). Interfacing finite elements with deep neural operators for fast multiscale modeling. *Computer Methods in Applied Mechanics and Engineering*, *402*, 115027. https://doi.org/10.1016/j.cma.2022.115027
[14] Zhang, D., Lu, L., Guo, L., & Karniadakis, G. E. (2019). Quantifying total uncertainty in physics-informed neural networks. *Journal of Computational Physics*, *397*, 108850. https://doi.org/10.1016/j.jcp.2019.07.048
[15] Tandale, S. B., Bamer, F., Markert, B., & Stoffel, M. (2022). Physics-based self-learning recurrent neural network for viscoplastic FEM response. *Computer Methods in Applied Mechanics and Engineering*, *401*, 115668. https://doi.org/10.1016/j.cma.2022.115668
[16] Versino, D., Tonda, A., & Bronkhorst, C. A. (2017). Data driven modeling of plastic deformation. *Computer Methods in Applied Mechanics and Engineering*, *318*, 981–1004. https://doi.org/10.1016/j.cma.2017.02.016
[17] Gorji, M. B., Mozaffar, M., Heidenreich, J. N., Cao, J., & Mohr, D. (2020). On the potential of recurrent neural networks for modeling path dependent plasticity. *Journal of the Mechanics and Physics of Solids*, *143*, 103972. https://doi.org/10.1016/j.jmps.2020.103972
[18] Forrester, A., Sobester, A., & Keane, A. (2008). *Engineering design via surrogate* modelling*: A practical guide*. Wiley. https://doi.org/10.1002/9780470770801

[19] Dyyak, I. I., & Prokopyshyn, I. I. (2010). Domain decomposition schemes for frictionless multibody contact problems of elasticity. In *Numerical Mathematics and Advanced Applications 2009* (pp. 301–308). Springer. https://doi.org/10.1007/978-3-642-11795-4_31
[20] COMSOL AB. (2023). Sheet Metal Forming. In *COMSOL Multiphysics Application Library, Nonlinear Structural Materials Module* (v6.2). https://www.comsol.com/model/sheet-metal-forming-11208
[21] Fazily, P., & Yoon, J. W. (2023). Machine learning-driven stress integration method for anisotropic plasticity in sheet metal forming. *International Journal of Plasticity*, *166*, 103642. https://doi.org/10.1016/j.ijplas.2023.103642
[22] Niu, S., Zhang, E., Bazilevs, Y., & Srivastava, V. (2023). Modeling finite-strain plasticity using physics-informed neural network and assessment of the network performance. *Journal of the Mechanics and Physics of Solids*, *172*, 105177. https://doi.org/10.1016/j.jmps.2022.105177
[23] Munzone, F., Hazrati, J., Hakvoort, W., & van den Boogaard, T. (2024). Comparative study of artificial neural network and physics-informed neural network application in sheet metal forming. *Materials Research Proceedings*, *41*, 2278–2288. https://doi.org/10.21741/9781644903131-251

АПРОКСИМАЦІЙНЕ МОДЕЛЮВАННЯ ПРУЖНО-ПЛАСТИЧНОГО ЗГИНАННЯ ЛИСТОВОГО МЕТАЛУ: ПОРІВНЯЛЬНЕ ДОСЛІДЖЕННЯ АПРОКСИМАЦІЙНИХ МЕТОДІВ ІЗ ДІАГНОСТИЧНОЮ ПЕРЕВІРКОЮ ФІЗИЧНОЇ РЕГУЛЯРИЗАЦІЇ

Богдан Петровський
Кафедра прикладної математики,
Львівський національний університет імені Івана Франка,
вул. Університетська, 1, Львів, 79007, УКРАЇНА

РЕЗЮМЕ

Вступ. Згинання листового металу є ключовою технологічною операцією, після якої відбувається пружне відновлення форми (англ. springback) — часткове пружне повернення заготовки після зняття навантаження, яке спричиняє відхилення від цільової геометрії деталі. Багаторазові симуляції методом скінченних елементів (МСЕ; англ. FEM) є обчислювально затратними для широких параметричних досліджень. Роботу присвячено порівнянню підходів до апроксимаційного моделювання та оцінці діагностичної цінності перевірки фізичної узгодженості для виявлення фізично неправдоподібних моделей незалежно від того, чи покращує регуляризація саму точність.

Матеріали та методи. Набір даних із 39 568 симуляцій МСЕ сформовано в COMSOL Multiphysics 6.2 шляхом варіювання товщини листа, переміщення пуансона та модуля Юнга заготовки зі сплаву 6111-T4. П’ять класичних методів та три моделі нейронних мереж (базова модель, керована лише даними; модель з регуляризацією за законом Холломона з коректними параметрами; контрольна модель із навмисно неправильними параметрами) порівняно на 5 випадкових розбиттях даних. Додатково просканована чутливість діагностики до величини «неправильності» показника зміцнення в контрольній моделі — від істинного значення до хибного.

Результати. Класичні непараметричні методи перевершують нейронну апроксимаційну модель на щільній гладкій параметричній сітці: випадковий ліс досягає

$R^2 > 0{,}9999$ проти $R^2 \approx 0{,}999$ для нейронних моделей. Різниці в точності між трьома нейронними моделями статистично виявляються між seeds (парний *t*-тест), але дуже малі за величиною ($\Delta R^2 < 0{,}1$ відсоткового пункту). Натомість метрика фізичної узгодженості розділяє моделі на порядки: $R^2 = 0{,}999$ для коректної моделі проти $R^2 \approx -2{,}9$ для некоректної. Сканування чутливості показує різкий пороговий ефект, а не поступову деградацію: узгодженість залишається майже ідеальною, доки похибка показника зміцнення невелика, і різко руйнується після суттєвого відхилення.

Висновки. Стандартні показники точності є недостатніми для виявлення фізично неузгоджених нейронних моделей, а сам діагностичний сигнал має пороговий, а не поступовий характер. Метрика фізичної узгодженості є незалежним діагностичним критерієм, який доповнює стандартні показники точності.

Ключові слова: фізично-регуляризовані нейронні мережі; апроксимаційне моделювання; згинання листового металу; пружне відновлення форми; закон зміцнення Холломона; ансамблевий метод випадкових дерев рішень.

Received / Одержано	Revised / Доопрацьовано	Accepted / Прийнято	Published / Опубліковано
17 July, 2026	30 August, 2026	03 September, 2026	28 September, 2026